Sustainability in Environment
ISSN 2470-637X (Print) ISSN 2470-6388 (Online)
Vol. 11, No. 4, 2026
www.scholink.org/ojs/index.php/se

Original Paper

Effects of Urban Blue–Green Landscape Patterns on Carbon Sequestration in Chongqing's Central Urban Area: An XGBoost–SHAP Analysis

Xiaoyu Gao[1], Zhongsheng Chen[1*], Ling Zhang[1], Kai Xiong[1], & Li Wang[1]

[1] School of Geographical Sciences, China West Normal University, Nanchong, Sichuan, China

[*] Corresponding Author

Received: September 27, 2026 Accepted: September 19, 2026 Online Published: October 23, 2026

doi:10.22158/se.v12n4p47 URL: http://dx.doi.org/10.22158/se.v12n4p47

Abstract

Against the backdrop of the "Dual Carbon" goals, this study focused on the main urban area in Chongqing. With remote sensing, land use, meteorological data from 2000, 2010, and 2020 -- we used the CASA model to estimate vegetation net primary productivity, or NPP, which we compared to MODIS NPP products. By combining optimal scale analysis, landscape pattern indices, the XGBoost model and SHAP (the Shapley Additive exPlanations) interpretation methods, our study showed that the space relationship between the blue and green landscapes and how they help to reduce the amount of vegetation carbon sinks are associated with one another, not just by the space that the areas are in, but by these other ways. The results indicate that from 2000 to 2020, NPP in the study area showed an overall upward trend. High-value areas were primarily distributed in the peripheral mountains and continuous ecological spaces, while blue-green spaces in the central urban area and densely built river valleys exhibited greater fragmentation. Compared to the baseline model (M0) containing only elevation and slope, the extended model (M1) incorporating landscape pattern indices significantly improved cross-validation R^2 values: from 0.5954, 0.6248, and 0.5735 to 0.7996, 0.8031, and 0.7311 for the years 2000, 2010, and 2020, respectively.SHAP analysis revealed that among the selected predictors, elevation contributed the most. PLAND (Percentage of Landscape) demonstrated a significant predictive contribution across all three years, whereas the roles of ED (Edge Density), SPLIT (Splitting Index), and AI (Aggregation Index) varied interannually. Nonlinear responses and reference thresholds were identified for elevation, slope, PLAND, LPI (Largest Patch Index), and their contributions to NPP prediction; however, SHAP contributions do not imply direct causal effects. The study concludes that topographic backgrounds, combined with the area, fragmentation, and

connectivity of blue-green spaces, collectively correlate with spatial variations in NPP within mountainous cities. These findings provide a reference for optimizing ecological spaces and enhancing vegetation carbon sink potential in the main urban area of Chongqing.

Keywords

urban blue–green landscape, optimal scale, landscape pattern, carbon sequestration, Chongqing central urban area, net primary productivity

1. Introduction

The continued rise in greenhouse gas emissions, especially carbon dioxide (CO_2), has contributed to global warming [1] and more frequent extreme weather events, posing serious environmental and social challenges. In response to climate change, the Paris Agreement, which entered into force in 2016, emphasized the need to reduce greenhouse gas emissions and strengthen carbon sinks. At the 75th Session of the United Nations General Assembly, China announced its goals of achieving carbon peaking and carbon neutrality. Cities cover only about 3% of the world's land area but are home to more than half of the global population and account for over 70% of carbon emissions [2]. These figures highlight the importance of promoting low-carbon urban development in meeting China's carbon reduction targets [3].

Urban blue–green landscapes (UBGLs) consist of green spaces and water bodies that are either preserved or developed as cities expand. These landscapes encompass natural, semi-natural, and artificial environments and form an essential part of urban ecosystems [4]. Urban vegetation plays an important role in carbon sequestration, with studies suggesting that green spaces can offset 28–37% of CO_2 emissions [5]. Water bodies, such as wetlands, rivers, and lakes, also contribute to carbon storage. Wetlands, for example, occupy only 5–8% of the global land area but hold approximately 20–30% of the world's soil carbon [6]. Beyond carbon storage, blue–green spaces may help reduce emissions by alleviating urban heat-island effects, regulating local temperatures, and encouraging more sustainable transport options [7]. Together, these functions make UBGLs an important part of urban carbon management, both through carbon sequestration and through their potential to reduce emissions indirectly [8].

Carbon sequestration in urban blue–green spaces has been studied using field surveys, remote sensing, and various modeling approaches [9–12]. These methods have been applied to estimate carbon storage and sequestration potential in forests, grasslands, and urban green spaces [13–16]. Among them, remote sensing has been widely used to estimate vegetation net primary productivity (NPP) at both regional and urban scales [17]. Researchers have also explored the factors influencing carbon sequestration, focusing on climate and environmental conditions, including temperature, precipitation, and soil properties [18,19], as well as land use patterns and urban tree species [20,21]. For example, Rani et al. [22] reported that an increase in forest area was associated with higher NPP in urban environments. Li et al. [23] found that converting cropland into forest and grassland could improve ecosystem carbon

sequestration. More recently, studies in landscape ecology have begun to examine how the spatial arrangement of different landscape elements influences carbon sequestration [24,25]. Several studies have explored the relationship between landscape patterns and carbon sequestration, suggesting that changes in landscape configuration may help improve carbon-sink capacity [26,27]. However, these relationships are often assessed using Pearson or Spearman correlation analysis [28]. Multiple linear regression [29,30] and geographically weighted regression are also commonly used, but they may not adequately capture nonlinear relationships and interactions among variables [31]. To address these limitations, machine-learning methods such as random forests, boosted regression trees, and extreme gradient boosting have been applied in carbon-sequestration studies [32]. Although these models often achieve good predictive accuracy, their complex structures make it difficult to explain how individual variables affect the results. This has led to the use of interpretation methods such as Local Interpretable Model-Agnostic Explanations (LIME) and SHapley Additive exPlanations (SHAP), which help identify important predictors and explain model outputs [33]. LIME mainly explains individual predictions, whereas SHAP measures the contribution of each variable and allows both local and global interpretation [34]. SHAP is therefore useful for examining how UBGL spatial patterns relate to carbon-sequestration performance. Nevertheless, many existing studies have focused mainly on landscape-pattern metrics [35,36], with less attention given to the combined influence of climatic factors, environmental conditions, and landscape configuration.

This study focused on Chongqing's central urban area to investigate how urban blue–green landscape (UBGL) patterns, environmental conditions, and climatic factors relate to carbon sequestration. Three questions guided the analysis: (1) How are UBGL patterns related to carbon-sequestration performance? (2) How do environmental conditions, climate, and landscape patterns affect urban carbon sinks through nonlinear relationships? (3) Which of these factors contribute most to carbon sequestration?

2. Data and Methods

The analysis involved four main components: blue–green space identification, spatial scale selection, landscape pattern analysis, and carbon sequestration assessment. Data from 2000, 2010, and 2020 were used to limit the effects of differences in image quality and unusual climatic conditions in individual years. Land-use and remote-sensing data were used to map blue–green spaces in Chongqing's central urban area. Forests and grasslands were classified as green spaces, while rivers, lakes, and reservoirs were treated as blue spaces. The analytical scale was selected by comparing landscape metrics calculated at different grain sizes and moving-window sizes. At the class level, landscape structure was described using metrics of area, shape, fragmentation, aggregation, and connectivity. Vegetation net primary productivity (NPP) was estimated using the CASA model, and the results were evaluated against MODIS NPP products. The relationships between NPP and landscape patterns, environmental conditions, and climatic factors were then examined using XGBoost and SHAP, with particular attention to nonlinear responses and the relative importance of individual variables.

2.1 Study Area

Chongqing lies in southwestern China, in the upper reaches of the Yangtze River, between 28°10′–32°13′ N and 105°17′–110°11′ E (Figure 1). It covers an area of about 82,400 km² and has a humid subtropical monsoon climate, with an average annual precipitation of 1,136.5 mm. The terrain consists mainly of mountains and hills, crossed by the Yangtze and Jialing rivers. This study focused on 22 districts and counties in Chongqing's central urban region, covering the central city, western Chongqing, and the eastern new urban area. The region has experienced considerable population growth and urban development, with blue–green spaces distributed across a diverse landscape. The Yangtze and Jialing rivers form the main blue ecological corridors, while the Jinyun, Zhongliang, Nanshan, and Tongluo mountains provide important green ecological barriers. However, continued urban expansion has led to the fragmentation of blue–green spaces and reduced connectivity between them, which may affect their capacity for carbon sequestration.

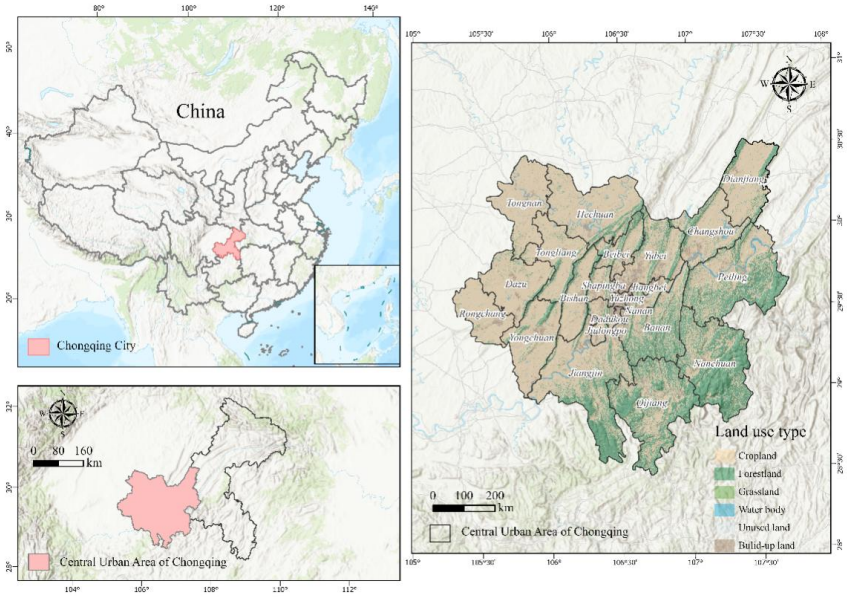


Figure 1. Location of the Study Area

2.2 Data Sources and Preprocessing

The datasets used in this study included land use, meteorological variables, vegetation type, and NPP. The 30-m China Land Cover Dataset (CLCD) [37] was used, in which land cover is classified into nine categories: cropland, forest, shrubland, grassland, water, snow and ice, barren land, impervious surface, and wetland. The land-use data were reclassified in ArcGIS. Forest, grassland, wetland, and shrubland were categorized as green space, and water bodies were categorized as blue space. This procedure produced UBGL distribution maps for Chongqing's central urban area in the three study years (Figure 2).

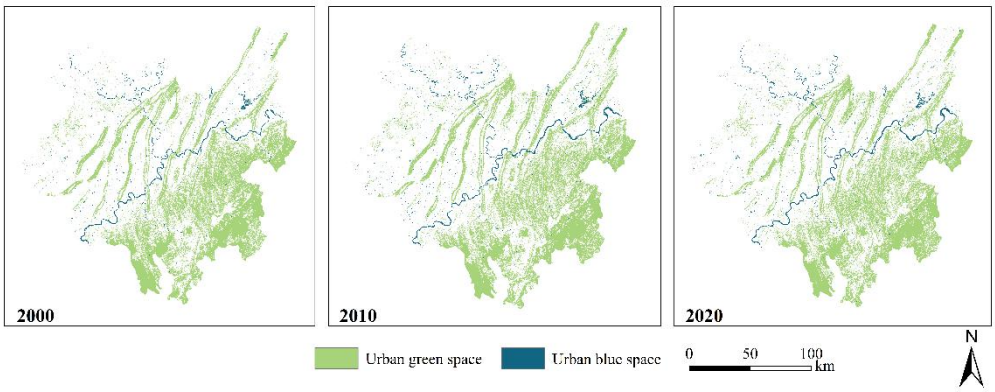


Figure 2. Distribution of Urban Blue–Green Spaces

Meteorological data, including monthly temperature, precipitation, and solar radiation, were obtained from the Geographic Remote Sensing Ecology Network (http://www.gisrs.cn/). Kriging interpolation was performed in ArcGIS 10.7, and monthly rasters were aggregated into annual datasets for 2000, 2010, and 2020. All layers were resampled to 30 m resolution and clipped to the study area.

Vegetation-type maps for the three years were obtained from the same source and processed to a consistent 30 m resolution. NDVI data were derived from Landsat imagery through Google Earth Engine (GEE; https://earthengine.google.com/). Following cloud masking and median compositing, monthly NDVI images were generated and stacked in ENVI 5.3 to construct annual NDVI time series.

The MOD17A3HGF NPP product, accessed through GEE, was used to validate CASA-derived NPP estimates. This MODIS Collection 6 dataset has a spatial resolution of 500 m and has undergone stage-3 validation. NPP data for 2000, 2010, and 2020 were extracted and processed in ArcGIS 10.7 through clipping and annual averaging to obtain annual mean NPP maps for the study area.

2.3 Methods

2.3.1 NPP Estimation Using the CASA Model

This study employed the Carnegie–Ames–Stanford Approach (CASA) model, a process-based light-use-efficiency model originally proposed by Potter et al. [38]. The model uses remotely sensed data to describe temporal changes in water, carbon, and nitrogen fluxes in terrestrial ecosystems and is particularly suitable for regional-scale NPP estimation. In the CASA framework, net primary productivity is expressed as the product of absorbed photosynthetically active radiation (APAR) and actual light-use efficiency (ε):

$$NPP(x,t) = APAR(x,t) \times \varepsilon(x,t) \quad (1)$$

In Equation (1), NPP(x,t) denotes the net primary productivity of pixel x in month t (g C m^{-2} $month^{-1}$), APAR(x,t) is the absorbed photosynthetically active radiation (MJ m^{-2} $month^{-1}$), and ε(x,t) is the actual light-use efficiency (g C MJ^{-1}).

2.3.2 Spatial Pattern Metrics of Urban Blue–Green Landscapes

Class-level metrics were used to characterize the spatial patterns of UBGLs (Table 1), with an emphasis

on their overall configuration. The selected metrics described the proportion, shape complexity, aggregation, fragmentation, and connectivity of blue–green spaces. UBGL patterns in 2000, 2010, and 2020 were calculated using FRAGSTATS 4.3. Given the spatial heterogeneity and scale dependence of urban blue–green landscapes [39], the choice of analytical scale can affect the results. Data from 2020 were used to determine a suitable scale for Chongqing's central urban area. The land-cover map was resampled in ArcGIS to produce raster datasets with grain sizes from 30 to 250 m, at 10-m intervals. By comparing the responses of landscape metrics to changes in grain size, 80 m was selected for further analysis. Moving-window size was then examined by fitting semivariograms to individual landscape metrics and calculating their nugget-to-sill ratios. A lower ratio generally indicates stronger spatial dependence. Based on these comparisons, a 400-m moving window was chosen to characterize the spatial patterns of UBGLs.

Table 1. Landscape Metrics Used to Characterize Urban Blue–green Landscape Patterns

Level	Metric	Formula	Definition
Class	Percentage of landscape (PLAND)	$PLAND = \frac{\sum_{j-1}^{n} a_{ij}}{A}$	Proportional abundance of the corresponding patch type in the landscape
	Largest patch index (LPI)	$LPI = \frac{\max(a_{ij})}{A}$	A simple measure of landscape dominance
	Edge density (ED)	$ED = \frac{E}{A}$	Total length of all edges involving the corresponding patch type divided by total landscape area
	Landscape shape index (LSI)	$LSI = \frac{0.25E}{\sqrt{A}}$	A standardized measure of total edge or edge density that corrects for differences in landscape size
	Aggregation index (AI)	$AI = \left[\frac{g_{ij}}{\max \rightarrow g_{ij}}\right](100)$	Frequency with which patches of the same type occur adjacent to one another
	Splitting index (SPLIT)	$SPLIT = \frac{A^2}{\sum_{j=1}^{n} a_{ij}^2}$	Square of total landscape area divided by the sum of squared patch areas

Level	Metric	Formula	Definition
	Patch cohesion index (COHESION)	$COHESION = [1 - \frac{\sum_{j=1}^{m} P_{ij}}{\sum_{j=1}^{m} P_{ij}\sqrt{a_{ij}}}][1 - \frac{1}{\sqrt{A}}]^{-1}$, $(0 < COHESION < 100)$	Physical connectedness of the corresponding patch type

2.3.3 XGBoost and SHAP Models

2.3.3.1 Extreme Gradient Boosting (XGBoost)

XGBoost, proposed by Chen and Guestrin [40], is an extreme gradient-boosted tree algorithm that combines supervised and ensemble learning. The model is optimized iteratively by fitting successive learners to the residual structure in the training data. Its objective function generally consists of a training-loss term and a regularization term, as shown in Equation (2):

$$Obj(\theta) = L(\theta) + \Omega(\theta) \quad (2)$$

where L is the training-loss function and Ω is the regularization term. The loss function measures predictive error on the training data, whereas regularization controls model complexity and helps reduce overfitting.

1) Dataset construction

Six datasets were constructed using patch-level and class-level metrics and their corresponding NPP values for 2000, 2010, and 2020. Taking 2020 as an example, 80,000 points were randomly generated within the study area using the random-sampling tool in ArcGIS 10.7. To ensure a sufficiently large and spatially balanced class-level dataset, points outside blue–green spaces were excluded.

2) Hyperparameter optimization

A tree-structured Parzen estimator (TPE), which is a Bayesian optimization algorithm, was used to tune the XGBoost hyperparameters. The principal parameters optimized were n_estimators, max_depth, and learning_rate.

3) Model validation

Model performance was assessed using three metrics: mean absolute error (MAE), root mean square error (RMSE), and the coefficient of determination (R^2). A higher R^2 value, approaching 1, generally indicates a better fit [41]. To examine model generalizability, we also performed 10-fold cross-validation. The data were randomly divided into 10 approximately equal groups, with nine used for training and the remaining one for validation. This process was repeated 10 times, allowing each

group to serve as the validation set once. The average performance across the 10 folds was then calculated to assess the model's predictive ability [42].

2.3.3.2 SHapley Additive exPlanations (SHAP)

Conventional machine-learning models are often regarded as “black-box” systems because their internal decision processes are difficult to interpret. The development of explainable machine learning has enabled these opaque models to be analyzed more transparently. SHAP is commonly coupled with XGBoost and has become an important approach for identifying and interpreting the drivers of model predictions [34]. Derived from Shapley values in cooperative game theory, SHAP quantifies the contribution of each predictor to a model output and thereby provides local explanations for individual predictions [33]. By examining the sign and magnitude of SHAP values, the positive or negative effect of each predictor and its contribution to model predictions can be assessed. For a model F with input x, SHAP assumes that the model output can be decomposed into the sum of individual feature contributions:

$$f(x) = \phi_0 + \sum_{i=1}^{M} \phi_i \quad (3)$$

Here, ϕ_0 is the baseline value, typically the mean prediction across all samples, and ϕ_i is the contribution of the ith feature to a given prediction. SHAP defines each feature contribution as the weighted mean of its marginal contribution.

3. Results

3.1 Spatial Patterns of Urban Blue–Green Landscapes

Class-level landscape metrics showed that the spatial distribution of blue–green spaces in Chongqing's central urban area changed relatively little between 2000 and 2020 (Figure 3), although some local differences were evident. SPLIT values were generally higher in river valleys and densely built-up areas, where blue–green spaces were more fragmented. Lower values occurred mainly in the surrounding mountains and continuous ecological areas. In the southern and southeastern mountains, high PLAND and LPI values reflected the large extent of blue–green spaces and the presence of dominant patches. By comparison, the central urban area and river corridors had higher ED and LSI values, indicating more irregular patch boundaries associated with terrain and urban development. COHESION and AI were higher in the continuous green spaces of the south, where patches were more connected and aggregated. These patterns reveal a clear contrast between the relatively intact landscapes of the surrounding mountains and the fragmented blue–green spaces of the urban core and river valleys. Despite some improvement in landscape connectivity over the study period, fragmentation remained apparent in areas affected by urban expansion.

3.2 NPP Estimates and Validation

Figure 4 shows the spatial variation in NPP across Chongqing’s central urban area between 2000 and 2020. NPP varied considerably across the region but generally increased over time. In 2000, most areas had low to moderate NPP, with higher values mainly occurring in the southern and eastern mountains.

By 2010, areas with high NPP had become more widespread, particularly in the surrounding mountains and hills. This pattern continued in 2020, with further increases in the southern and southeastern regions, while densely built-up areas maintained relatively low NPP. The observed changes point to an improvement in vegetation productivity and potential carbon sequestration over the study period. CASA estimates were closely correlated with MODIS NPP(Figure 5), with R^2 values of 0.890, 0.891, and 0.842 for 2000, 2010, and 2020, respectively. Although the agreement was slightly weaker in 2020, the correlation remained high. Regression slopes below 1 also revealed differences between the two datasets, with CASA tending to produce higher estimates at higher NPP levels. These comparisons suggest that CASA-derived NPP is suitable for examining long-term changes in vegetation productivity in the study area.

3.3 XGBoost–SHAP Analysis

3.3.1 Overall Model Performance

The data were randomly split into training (80%) and testing (20%) sets for XGBoost modeling, with 10-fold cross-validation used to evaluate model stability(Table 2). Across the three study years, test-set R^2 ranged from 0.839 to 0.893, while cross-validation R^2 ranged from 0.848 to 0.897. The consistently high R^2 values suggest that XGBoost performed well in predicting NPP from the selected explanatory variables, including their nonlinear relationships.

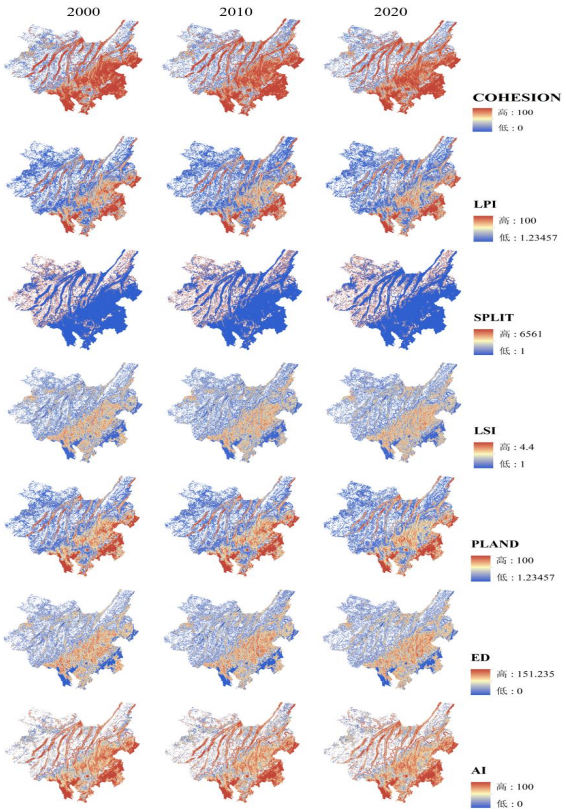


Figure 3. Spatial Distribution of Class-level Landscape Metrics in Central Chongqing in 2000, 2010, and 2020

3.3.2 SHAP Summary Analysis

Adding landscape pattern metrics improved the XGBoost model's ability to predict NPP in Chongqing's central urban area(Figure 6)(Figure 7). The baseline model (M0), based only on elevation and slope, had CV-R^2 values of 0.5954, 0.6248, and 0.5735 in 2000, 2010, and 2020, respectively. With landscape metrics included (M1), these values rose to 0.7996, 0.8031, and 0.7311, corresponding to increases of 0.2042, 0.1783, and 0.1576. Test-set RMSE decreased by 28.9%, 22.9%, and 20.1%, while MAE fell by 29.9%, 22.0%, and 18.1% across the three years. The improvement was greatest in 2000 and smallest in 2020, indicating that the additional predictive value of landscape metrics differed over time.

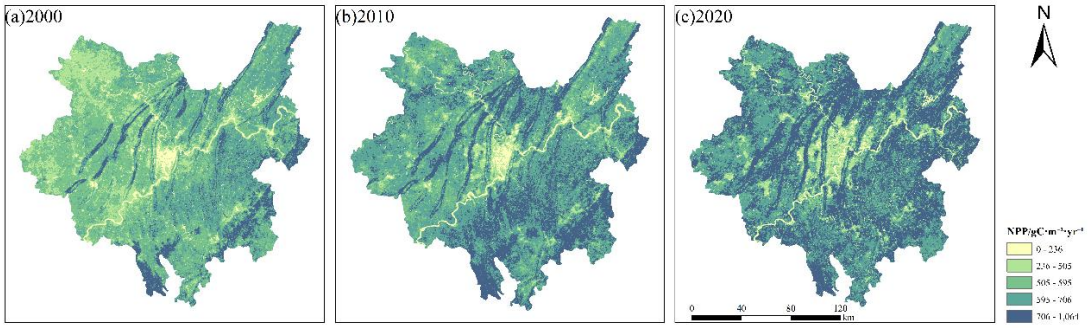


Figure 4. Spatial Distribution of NPP in Chongqing's Central Urban Area

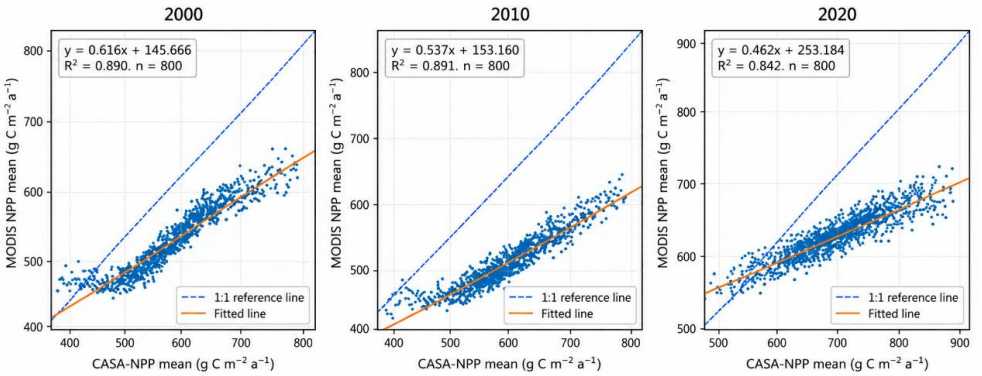


Figure 5. Scatter Plots Comparing CASA-estimated and MODIS-derived NPP

Table 2. Overall Model Performance

Year	Dataset	RMSE	MAE	R^2	10-fold cross-validation R^2
2000	Training dataset	24.520	18.326	0.969	0.897
	Testing dataset	46.621	33.378	0.890	
2010	Training	28.062	20.507	0.962	0.891

	dataset				
	Testing dataset	48.994	36.047	0.893	
2020	Training dataset	24.853	17.990	0.970	0.848
	Testing dataset	55.597	40.606	0.839	

SHAP analysis revealed differences in the importance of NPP predictors across the three study years. Elevation remained the leading variable throughout 2000–2020, with a wide range of SHAP values reflecting its strong influence on model predictions. In 2000, PLAND, ED, and slope were also important. Higher PLAND values generally corresponded to positive SHAP contributions, while ED tended to show negative values at higher levels. By 2010, SPLIT had become more influential, although ED, slope, and PLAND still played important roles. In 2020, slope ranked second, followed by PLAND. The contribution of PLAND remained largely positive, whereas AI and COHESION showed mixed positive and negative SHAP values.

Elevation consistently had the highest importance, and PLAND maintained a relatively stable contribution. In comparison, the importance of ED, SPLIT, and AI changed across years. These findings, together with the improvement in model accuracy after adding landscape metrics, indicate that landscape composition and spatial arrangement provide useful information for NPP prediction beyond terrain factors alone.

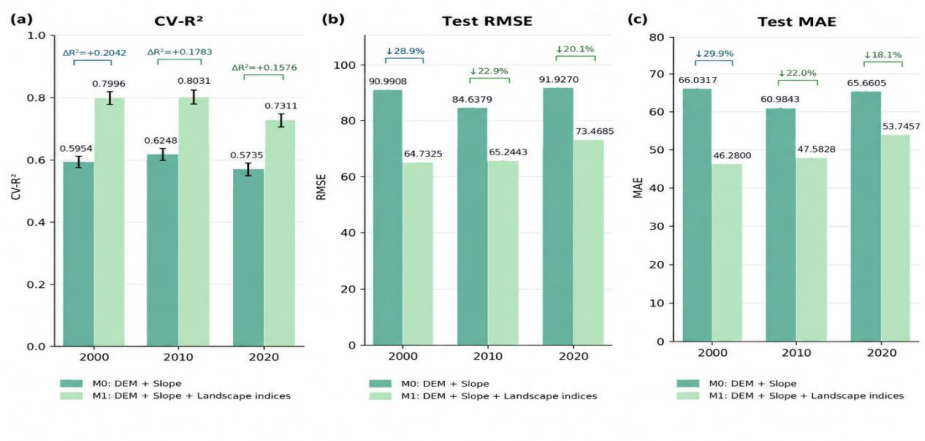


Figure 6. Comparison of Prediction Performance between M0 and M1 for 2000, 2010, and 2020

3.3.3 Feature Dependence Analysis

SHAP dependence plots showed nonlinear relationships between NPP predictions and terrain and landscape metrics in Chongqing's central urban area, with thresholds varying across the three years(Figure 8)(Figure 9). For elevation, the estimated thresholds were 316, 300, and 311 m in 2000,

2010, and 2020, respectively. SHAP values were mostly negative at lower elevations but increased sharply as elevation rose, before leveling off above 400–500 m. Slope followed a similar pattern, with thresholds of 3.17°, 2.49°, and 2.66° across the three years. Its SHAP values increased rapidly at gentle slopes and became relatively stable at steeper gradients.

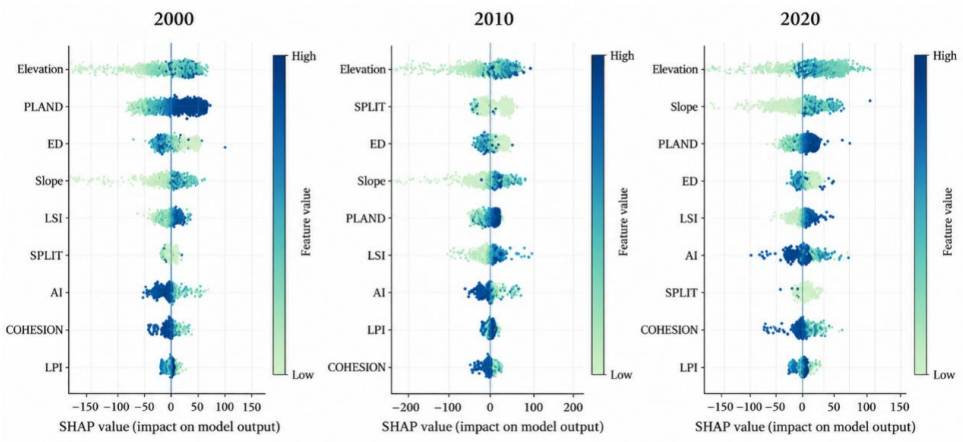


Figure 7. SHAP Summary Plots of M1 Model Features for 2000, 2010, and 2020

PLAND showed thresholds of 57.42%, 86.19%, and 91.78% in 2000, 2010, and 2020, respectively. Above these values, SHAP contributions were mostly positive, suggesting that the transition to positive contributions occurred at higher PLAND levels over time. For LPI, the thresholds were 77.59%, 83.41%, and 71.88%, with larger values generally corresponding to positive SHAP contributions. ED displayed a different pattern. In 2000 and 2010, SHAP values dropped sharply before leveling off, with thresholds of 37.27 and 38.08. In 2020, they initially declined and then increased slightly, with the turning point occurring around 76.17. LSI had thresholds of 1.75, 2.28, and 2.12 across the three years. Its SHAP values tended to increase with LSI, although some fluctuations were observed at higher values.

AI showed thresholds of 77.70%, 85.35%, and 65.58% in 2000, 2010, and 2020, respectively. Its SHAP values first decreased and then increased in 2000 and 2020, while a downward trend was observed in 2010. For SPLIT, most SHAP values were close to zero, and relatively few samples had high SPLIT values, making the relationship difficult to interpret with confidence. COHESION had thresholds of 88.86%, 89.17%, and 89.45% across the three years. Its SHAP values generally decreased as COHESION increased, although the pattern became less consistent at higher values.

Elevation and slope showed clear changes in SHAP contributions at lower values. Higher PLAND and LPI values were generally linked to positive contributions to predicted NPP. In comparison, the SHAP patterns of other landscape metrics differed across the three years, both in direction and magnitude.

4. Discussion

4.1 Key Determinants of Carbon-Sequestration Performance

Including landscape metrics improved the predictive performance of the XGBoost model for NPP in Chongqing's central urban area. The baseline model (M0), using only elevation and slope, achieved cross-validated R^2 values of 0.5954, 0.6248, and 0.5735 for 2000, 2010, and 2020, respectively. After landscape metrics were included, these values increased to 0.7996, 0.8031, and 0.7311. Test-set RMSE was reduced by 28.9%, 22.9%, and 20.1% across the three years, while MAE decreased by 29.9%, 22.0%, and 18.1%. The results indicate that landscape configuration contains useful information for predicting NPP that is not captured by elevation and slope alone.

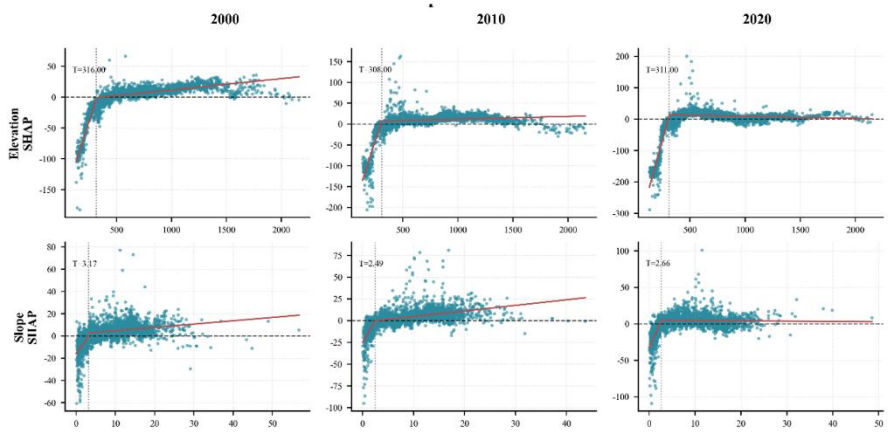


Figure 8. SHAP Dependence Plots of M0 Model Features

Elevation was the leading predictor of NPP across all three years. PLAND, ED, and slope were important in 2000, while SPLIT gained importance in 2010. In 2020, slope and PLAND ranked second and third. These shifts indicate changes in the relative importance of landscape metrics, although SHAP does not establish causality [34]. The importance of terrain reflects Chongqing's mountainous landscape, where extensive ecological areas occur mainly in peripheral mountains [24]. PLAND remained influential, and higher LPI values were generally linked to positive SHAP contributions, consistent with previous studies [15,16]. ED and LSI showed nonlinear patterns, while the contributions of SPLIT, AI, and COHESION varied across years [26,56]. Landscape metrics thus provided useful information beyond topography. Their smaller improvement in predictive performance in 2020 may be related to urban expansion and changes in landscape structure, although this requires further study.

4.2 Mechanisms Underlying Carbon Sequestration

The relationships between environmental factors and NPP were nonlinear, as reported in previous studies [30,46]. Increasing vegetation cover generally favors carbon sequestration, although the response may vary with vegetation structure and local growing conditions.

Adequate precipitation generally supports vegetation growth by alleviating water stress, although

excessive rainfall can lead to waterlogging and limit root activity [47]. Temperature is closely related to photosynthesis and respiration, while elevation and slope shape vegetation growth conditions through differences in local climate, terrain, and human disturbance [48–50]. As a result, conditions favorable for vegetation productivity may vary considerably across mountainous areas. Regarding landscape patterns, PLAND showed a positive relationship with NPP in all three study years, suggesting that areas with a greater proportion of blue–green space tended to have higher vegetation productivity. LPI also showed positive contributions to predicted NPP at higher values. Compared with small, isolated patches, large and continuous patches may offer more stable conditions for vegetation growth and be less exposed to edge disturbances [39,52–55].

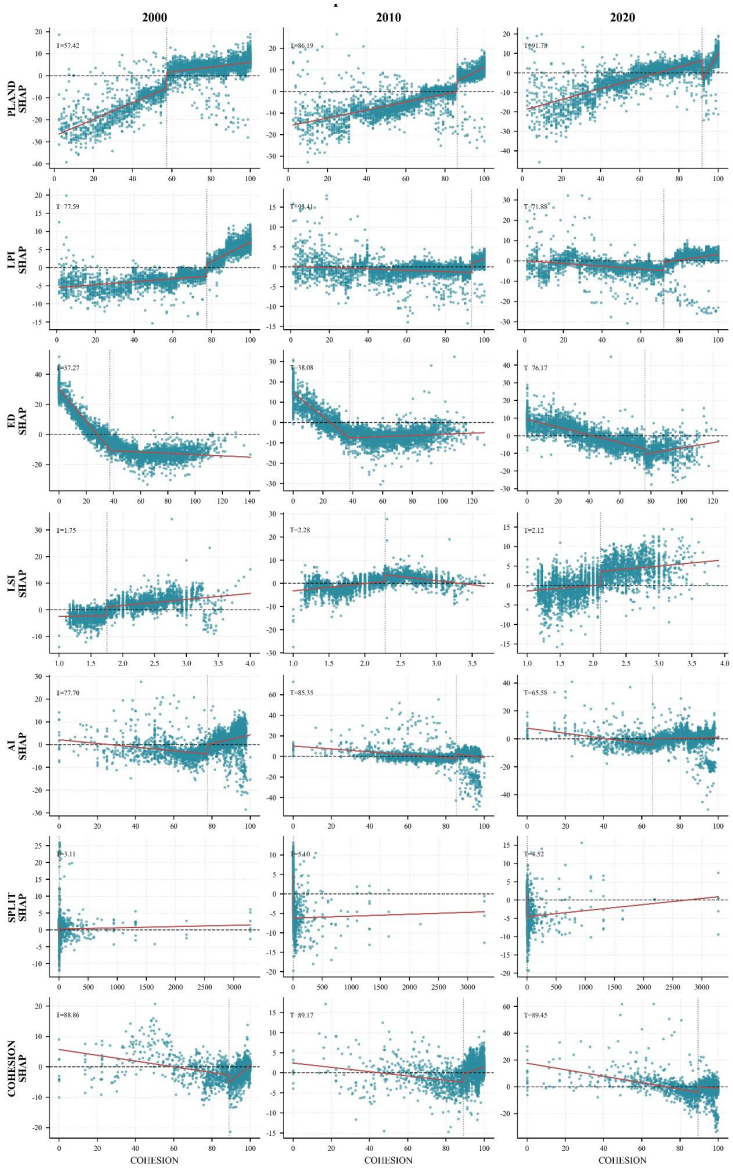


Figure 9. SHAP Dependence Plots of Landscape Pattern Metrics in the M1 Model

The relationships between landscape configuration and NPP were less straightforward. Both ED and LSI exhibited nonlinear patterns, indicating that the effects of patch boundaries and shape complexity on vegetation productivity may vary across different landscape conditions. A certain degree of shape complexity may support ecological exchanges, whereas highly fragmented landscapes are more likely to experience edge disturbance and loss of patch integrity. ED was generally negatively associated with predicted NPP, suggesting that landscapes with more extensive patch boundaries may be less favorable for vegetation growth. The response of LSI also varied, indicating that more complex patch shapes do not always correspond to higher carbon sequestration [56,58]. SPLIT, AI, and COHESION describe landscape division, aggregation, and connectivity, respectively. A higher SPLIT value generally indicates a more divided landscape, which may weaken ecological continuity. By comparison, aggregated patches may be better able to maintain relatively continuous green spaces. Although connectivity can support ecological exchanges between patches, its relationship with NPP is likely to vary with vegetation conditions, patch location, and surrounding land use [61,62]. In Chongqing's central urban area, the mountainous landscape, the Yangtze and Jialing rivers, and ongoing urban development have shaped a spatial pattern in which large, continuous ecological areas coexist with smaller, fragmented urban green spaces. These findings indicate that NPP is related not only to the amount of blue–green space but also to how these spaces are arranged and the environmental conditions in which they occur.

4.3 Implications for Blue–Green Space Optimization and Management

For Chongqing's central urban area, improving blue–green spaces requires more than simply expanding their coverage. Greater attention should be paid to conserving existing green spaces, protecting large patches, and improving their spatial arrangement. Areas with high NPP, particularly the surrounding mountains, continuous forests, and large urban parks, should be protected from further disturbance. Road construction and urban expansion need to be carefully managed to avoid breaking up large blue–green patches. Maintaining ecological corridors and restoring important habitat connections may also help preserve landscape continuity. In highly urbanized areas and river valleys, small parks, riparian buffers, roadside vegetation, and the restoration of unused land could provide additional green space and improve connectivity between existing patches. These measures may also increase PLAND and, where space permits, support the formation of larger patches. The thresholds observed for PLAND and LPI, however, are based on statistical relationships in the model and should not be treated as fixed targets for urban planning. Similarly, higher values of ED, LSI, AI, or COHESION do not necessarily indicate better ecological conditions. Planning decisions should therefore account for local terrain, land use, and vegetation quality rather than focusing on individual landscape metrics. Reducing unnecessary fragmentation and strengthening connections between major ecological areas may be more useful in practice. Regular monitoring of landscape patterns and NPP could also be included in urban renewal and territorial spatial planning. Comparing results over time would help determine whether these interventions lead to measurable improvements in ecological conditions and carbon sequestration.

4.4 Limitations and Future Directions

Remote-sensing data used in this study were obtained from Landsat 5, 7, and 8. Differences in sensor characteristics, particularly spectral band configurations and spatial resolution, may have affected the consistency of land-surface information across the study years. Such differences could also introduce uncertainties into the landscape analysis. Furthermore, this study mainly examined landscape patterns and broad environmental factors, while vegetation types, community structure, and species composition were not explicitly considered. This may restrict our understanding of the ecological processes underlying carbon sequestration. Urban blue–green landscapes also have complex three-dimensional structures, but their role in carbon sequestration has received relatively little attention [64]. Future studies could consider three-dimensional landscape characteristics [65] and spatial network topology [66] to better describe urban blue–green landscape configurations and examine their relationships with carbon sequestration. Finally, although XGBoost–SHAP was useful for identifying important variables and nonlinear relationships, the results should be interpreted as statistical associations rather than evidence of causality.

Future studies could build on this work in several ways. First, higher-resolution remote-sensing imagery and data from multiple sources could be used to improve blue–green space mapping and reduce uncertainty in carbon sequestration estimates. Second, examining landscape patterns at the regional scale alongside vegetation characteristics at the local scale may help clarify how the relationships between landscape structure and carbon sequestration vary with spatial scale. Further attention should also be given to interactions among environmental factors and how these relationships change over time. Finally, incorporating three-dimensional vegetation structure and spatial network characteristics could improve the representation of urban blue–green landscapes and provide further insight into their relationship with carbon sequestration.

5. Conclusions

This study examined how blue–green landscape patterns relate to net primary productivity (NPP) in Chongqing's central urban area in 2000, 2010, and 2020. The analysis combined spatial scale selection, CASA-based NPP estimation, and XGBoost–SHAP. NPP increased overall during the study period, with higher values mainly found in the surrounding mountains and larger, continuous ecological areas. Blue–green spaces in these areas were relatively well connected, while those in the urban core and river valleys showed greater fragmentation. Including landscape metrics increased the cross-validated R^2 from 0.5954 to 0.7996 in 2000, from 0.6248 to 0.8031 in 2010, and from 0.5735 to 0.7311 in 2020. This suggests that landscape configuration provides useful information for NPP prediction beyond topographic factors alone. SHAP analysis identified elevation as the leading predictor across all three years, with PLAND also showing a consistently strong contribution. In contrast, the influence of ED, SPLIT, and AI differed between years. Elevation and slope showed nonlinear relationships with predicted NPP, including noticeable threshold effects, while higher PLAND and LPI values were

generally linked to positive SHAP values. Overall, the results show that both terrain and landscape structure are closely related to the spatial distribution of NPP. Maintaining large ecological patches in mountainous areas, restoring fragmented green spaces in built-up areas, and improving connectivity in ways that reflect local terrain conditions may help enhance urban carbon-sink potential and promote low-carbon development.

References

[1] Abelson, P.H. Constraints on greenhouse gas emission. 1997, 278, 783-783.

[2] Change, I.C. The physical science basis. (No Title) 2013.

[3] Wang, Y.; Fang, X.; Yin, S.; Chen, W. Low-carbon development quality of cities in China: Evaluation and obstacle analysis. Sustainable Cities and Society 2021, 64, 102553.

[4] Yu, Z.; Yang, G.; Zuo, S.; Jørgensen, G.; Koga, M.; Vejre, H. Critical review on the cooling effect of urban blue-green space: A threshold-size perspective. Urban forestry & urban greening 2020, 49, 126630.

[5] Cheng, J.; Huang, C.; Gan, X.; Peng, C.; Deng, L. Can forest carbon sequestration offset industrial CO2 emissions? A case study of Hubei Province, China. Journal of Cleaner Production 2023, 426, 139147.

[6] Hu, H.; Wang, S.; Guo, Z.; Xu, B.; Fang, J. The stage-classified matrix models project a significant increase in biomass carbon stocks in China's forests between 2005 and 2050. Scientific Reports 2015, 5, 11203.

[7] Zhang, Y.; Meng, W.; Yun, H.; Xu, W.; Hu, B.; He, M.; Mo, X.; Zhang, L. Is urban green space a carbon sink or source?-A case study of China based on LCA method. Environmental Impact Assessment Review 2022, 94, 106766.

[8] Wolch, J.R.; Byrne, J.; Newell, J.P. Urban green space, public health, and environmental justice: The challenge of making cities 'just green enough'. Landscape and urban planning 2014, 125, 234-244.

[9] Chu, X.; Zhan, J.; Li, Z.; Zhang, F.; Qi, W. Assessment on forest carbon sequestration in the Three-North Shelterbelt Program region, China. Journal of Cleaner Production 2019, 215, 382-389.

[10] Qin, J.; Liu, P.; Martin, A.R.; Wang, W.; Lei, Y.; Li, H. Forest carbon storage and sink estimates under different management scenarios in China from 2020 to 2100. Science of The Total Environment 2024, 927, 172076.

[11] Wu, S.; Li, J.; Zhou, W.; Lewis, B.J.; Yu, D.; Zhou, L.; Jiang, L.; Dai, L. A statistical analysis of spatiotemporal variations and determinant factors of forest carbon storage under China's Natural Forest Protection Program. Journal of Forestry Research 2018, 29, 415-424.

[12] Zhao, Z.; Liu, G.; Mou, N.; Xie, Y.; Xu, Z.; Li, Y. Assessment of carbon storage and its influencing factors in Qinghai-Tibet Plateau. Sustainability 2018, 10, 1864.

[13] Ameray, A.; Bergeron, Y.; Valeria, O.; Montoro Girona, M.; Cavard, X. Forest carbon management: A review of silvicultural practices and management strategies across boreal, temperate

and tropical forests. Current Forestry Reports 2021, 7, 245-266.

[14] Ma, Q.; Kuang, W.; Liu, Z.; Hu, F.; Qian, J.; Liu, B.; Zhu, J.; Cao, C.; Wu, J.; Li, X. Spatial pattern of different component carbon in varied grasslands of northern China. Geoderma 2017, 303, 27-36.

[15] Shi, N.; Yu, Y.; Liang, S.; Ren, Y.; Liu, M. Effects of urban green spaces landscape pattern on carbon sink among urban ecological function areas at the appropriate scale: A case study in Xi'an. Ecological Indicators 2024, 158, 111427.

[16] Yuan, Y.; Guo, W.; Tang, S.; Zhang, J. Effects of patterns of urban green-blue landscape on carbon sequestration using XGBoost-SHAP model. Journal of Cleaner Production 2024, 476, 143640.

[17] Lee, J.-H.; Ko, Y.; McPherson, E.G. The feasibility of remotely sensed data to estimate urban tree dimensions and biomass. Urban Forestry & Urban Greening 2016, 16, 208-220.

[18] Fang, J.; Yu, G.; Liu, L.; Hu, S.; Chapin III, F.S. Climate change, human impacts, and carbon sequestration in China. Proceedings of the National Academy of Sciences 2018, 115, 4015-4020.

[19] Golub, A.; Sohngen, B.; Cai, Y.; Kim, J.; Hertel, T. Costs of forest carbon sequestration in the presence of climate change impacts. Environmental Research Letters 2022, 17, 104011.

[20] Beltrán-Sanz, N.; Raggio, J.; Gonzalez, S.; Dal Grande, F.; Prost, S.; Green, A.; Pintado, A.; Sancho, L.G. Climate change leads to higher NPP at the end of the century in the Antarctic Tundra: Response patterns through the lens of lichens. Science of the Total Environment 2022, 835, 155495.

[21] Marques, A.; Martins, I.S.; Kastner, T.; Plutzar, C.; Theurl, M.C.; Eisenmenger, N.; Huijbregts, M.A.; Wood, R.; Stadler, K.; Bruckner, M. Increasing impacts of land use on biodiversity and carbon sequestration driven by population and economic growth. Nature ecology & evolution 2019, 3, 628-637.

[22] Rani, V.; Schwing, P.T.; Jayachandran, P.; Preethy, C.; Sreelekshmi, S.; Joseph, P.; Nandan, S.B. Carbon stocks and sequestration rate in mangroves and its major influencing factors from highly urbanised port city, southern India. Journal of environmental management 2023, 335, 117542.

[23] Li, J.; Wang, Z.; Lai, C.; Wu, X.; Zeng, Z.; Chen, X.; Lian, Y. Response of net primary production to land use and land cover change in mainland China since the late 1980s. Science of the Total Environment 2018, 639, 237-247.

[24] Hu, C.; Wu, W.; Zhou, X.; Wang, Z. Spatiotemporal changes in landscape patterns in karst mountainous regions based on the optimal landscape scale: A case study of Guiyang City in Guizhou Province, China. Ecological Indicators 2023, 150, 110211.

[25] Jingmao, W.; Yifan, W.; Liyixuan, F.; Ting, S. Research on spatial pattern of green space in urban block units and optimization of carbon sink benefits of plant communities. Landscape Architecture 2024, 31, 37-45.

[26] Tang, Z.; Wang, Y.; Fu, M.; Xue, J. The role of land use landscape patterns in the carbon emission reduction: Empirical evidence from China. Ecological Indicators 2023, 156, 111176.

[27] Wang, K.; Zhang, C.; Chen, H.; Yue, Y.; Zhang, W.; Zhang, M.; Qi, X.; Fu, Z. Karst landscapes of China: patterns, ecosystem processes and services. Landscape Ecology 2019, 34, 2743-2763.

[28] Xu, X.; Wang, C.; Sun, Z.; Hao, Z.; Day, S. How do urban forests with different land use histories influence soil organic carbon? Urban Forestry & Urban Greening 2023, 83, 127918.

[29] Song, S.; Kong, M.; Su, M.; Ma, Y. Study on carbon sink of cropland and influencing factors: A multiscale analysis based on geographical weighted regression model. Journal of Cleaner Production 2024, 447, 141455.

[30] Wei, J.; Shen, M. Analysis of the efficiency of forest carbon sinks and its influencing factors—Evidence from China. Sustainability 2022, 14, 11155.

[31] Zhao, D.; Cai, J.; Shen, S.; Liu, Q.; Lan, Y. Nature-based solutions: Assessing the carbon sink potential and influencing factors of urban park plant communities in the temperate monsoon climate zone. Science of the Total Environment 2024, 950, 175347.

[32] Wang, Y.; Sheng, S.; Xiao, H. The cooling effect of hybrid land-use patterns and their marginal effects at the neighborhood scale. Urban Forestry & Urban Greening 2021, 59, 127015.

[33] Yang, C.; Chen, M.; Yuan, Q. The application of XGBoost and SHAP to examining the factors in freight truck-related crashes: An exploratory analysis. Accident Analysis & Prevention 2021, 158, 106153.

[34] Lundberg, S.M.; Lee, S.-I. A unified approach to interpreting model predictions. Advances in neural information processing systems 2017, 30.

[35] Jiang, Y.; Sun, Y.; Liu, Y.; Li, X. Exploring the correlation between waterbodies, green space morphology, and carbon dioxide concentration distributions in an urban waterfront green space: A simulation study based on the carbon cycle. Sustainable Cities and Society 2023, 98, 104831.

[36] Ren, Y.; Zhou, M.; Zhu, A.; Shi, S.; Zhu, H.; Chen, Y.; Li, S.; Fan, T. Evolution, reconfiguration and low-carbon performance of green space pattern under diverse urban development scenarios: A machine learning-based simulation approach. Ecological Indicators 2024, 169, 112945.

[37] Zhang, X.; Zhao, T.; Xu, H.; Liu, W.; Wang, J.; Chen, X.; Liu, L. GLC_FCS30D: the first global 30 m land-cover dynamics monitoring product with a fine classification system for the period from 1985 to 2022 generated using dense-time-series Landsat imagery and the continuous change-detection method. Earth System Science Data 2024, 16, 1353-1381.

[38] Potter, C.S.; Randerson, J.T.; Field, C.B.; Matson, P.A.; Vitousek, P.M.; Mooney, H.A.; Klooster, S.A. Terrestrial ecosystem production: A process model based on global satellite and surface data. Global biogeochemical cycles 1993, 7, 811-841.

[39] Wu, J. Effects of changing scale on landscape pattern analysis: scaling relations. Landscape ecology 2004, 19, 125-138.

[40] Chen, T.; Guestrin, C. Proceedings of the 22nd ACM SIGKDD international conference on knowledge discovery and data mining. 2016.

[41] Wang, S.; Zhou, Y.; You, X.; Wang, B.; Du, L. Quantification of the antagonistic and synergistic

effects of Pb2+, Cu2+, and Zn2+ bioaccumulation by living Bacillus subtilis biomass using XGBoost and SHAP. Journal of Hazardous Materials 2023, 446, 130635.

[42] Ye, M.; Zhu, L.; Li, X.; Ke, Y.; Huang, Y.; Chen, B.; Yu, H.; Li, H.; Feng, H. Estimation of the soil arsenic concentration using a geographically weighted XGBoost model based on hyperspectral data. Science of The Total Environment 2023, 858, 159798.

[43] Nie, Q.; Wu, G.; Li, L.; Man, W.; Ma, J.; Bao, Z.; Luo, L.; Li, H. Exploring scaling differences and spatial heterogeneity in drivers of carbon storage Changes: A comprehensive geographic analysis framework. Ecological Indicators 2024, 165, 112193.

[44] Wen, D.; He, N. Forest carbon storage along the north-south transect of eastern China: Spatial patterns, allocation, and influencing factors. Ecological Indicators 2016, 61, 960-967.

[45] Zheng, Y.; Du, S.; Sun, W.; Feng, C.; Su, Q. Spatiotemporal patterns of net regional productivity and its causes throughout Ordos, China. Environmental Science and Pollution Research 2024, 31, 22038-22054.

[46] Chen, B.; Liu, Y.; Li, Z.; Xu, C.; Hou, W. Spatiotemporal carbon sequestration by forests among counties and grids in China. Journal of Cleaner Production 2024, 468, 142971.

[47] Bai, Y.; Zhang, Y.; Hu, Y.; Lu, Y.; Tian, L.; Zhang, B. Water-stressed canopy stomatal behaviors across environmental gradients and ecosystems within an inland river basin. Water Resources Research 2025, 61, e2025WR039939.

[48] Nemani, R.R.; Keeling, C.D.; Hashimoto, H.; Jolly, W.M.; Piper, S.C.; Tucker, C.J.; Myneni, R.B.; Running, S.W. Climate-driven increases in global terrestrial net primary production from 1982 to 1999. science 2003, 300, 1560-1563.

[49] Zhao, M.; Running, S.W. Drought-induced reduction in global terrestrial net primary production from 2000 through 2009. science 2010, 329, 940-943.

[50] Cheng, Z.; Aakala, T.; Larjavaara, M. Elevation, aspect, and slope influence woody vegetation structure and composition but not species richness in a human-influenced landscape in northwestern Yunnan, China. Frontiers in Forests and Global Change 2023, 6, 1187724.

[51] Wei, D.; Qi, Y.; Ma, Y.; Wang, X.; Ma, W.; Gao, T.; Huang, L.; Zhao, H.; Zhang, J.; Wang, X. Plant uptake of CO2 outpaces losses from permafrost and plant respiration on the Tibetan Plateau. Proceedings of the National Academy of Sciences 2021, 118, e2015283118.

[52] McGarigal, K.; Cushman, S.A.; Ene, E. FRAGSTATS v4: spatial pattern analysis program for categorical and continuous maps. Computer software program produced by the authors at the University of Massachusetts, Amherst 2012, 15, 153-162.

[53] Fahrig, L. Effects of habitat fragmentation on biodiversity. Annual review of ecology, evolution, and systematics 2003, 34, 487-515.

[54] Turner, M.G. Landscape ecology in North America: past, present, and future. Ecology 2005, 86, 1967-1974.

[55] Turner, M.G. Disturbance and landscape dynamics in a changing world. Ecology 2010, 91,

2833-2849.

[56] Haddad, N.M.; Brudvig, L.A.; Clobert, J.; Davies, K.F.; Gonzalez, A.; Holt, R.D.; Lovejoy, T.E.; Sexton, J.O.; Austin, M.P.; Collins, C.D. Habitat fragmentation and its lasting impact on Earth's ecosystems. Science advances 2015, 1, e1500052.

[57] Uhl, J.H.; Leyk, S. Uncertainty prediction of built-up areas from global human settlement data in the United States based on landscape metrics. arXiv preprint arXiv:2205.09023 2022.

[58] Liao, W.; Guldmann, J.-M.; Hu, L.; Cao, Q.; Gan, D.; Li, X. Linking urban park cool island effects to the landscape patterns inside and outside the park: A simultaneous equation modeling approach. Landscape and Urban Planning 2023, 232, 104681.

[59] Delgado-Baquerizo, M.; Maestre, F.T.; Gallardo, A.; Bowker, M.A.; Wallenstein, M.D.; Quero, J.L.; Ochoa, V.; Gozalo, B.; García-Gómez, M.; Soliveres, S. Decoupling of soil nutrient cycles as a function of aridity in global drylands. Nature 2013, 502, 672-676.

[60] Mngadi, M.; Odindi, J.; Mutanga, O.; Sibanda, M. Estimating aboveground net primary productivity of reforested trees in an urban landscape using biophysical variables and remotely sensed data. Science of the Total Environment 2022, 802, 149958.

[61] Fahrig, L. Ecological responses to habitat fragmentation per se. Annual review of ecology, evolution, and systematics 2017, 48, 1-23.

[62] Zeller, K.A.; Lewison, R.; Fletcher Jr, R.J.; Tulbure, M.G.; Jennings, M.K. Understanding the importance of dynamic landscape connectivity. Land 2020, 9, 303.

[63] Fischer, J.; Lindenmayer, D.B. Landscape modification and habitat fragmentation: a synthesis. Global ecology and biogeography 2007, 16, 265-280.

[64] Yu, S.; Chen, Z.; Yu, B.; Wang, L.; Wu, B.; Wu, J.; Zhao, F. Exploring the relationship between 2D/3D landscape pattern and land surface temperature based on explainable eXtreme Gradient Boosting tree: A case study of Shanghai, China. Science of the total environment 2020, 725, 138229.

[65] Hu, Y.; Zhang, Q.; Hu, S.; Xiao, G.; Chen, X.; Wang, J.; Qi, Y.; Zhang, L.; Han, L. Research progress and prospects of ecosystem carbon sequestration under climate change (1992–2022). Ecological Indicators 2022, 145, 109656.

[66] Shen, Z.; Wu, W.; Tian, S.; Wang, J. A multi-scale analysis framework of different methods used in establishing ecological networks. Landscape and Urban Planning 2022, 228, 104579.